Impurity powder injection experiments in the Large Helical Device

F. Nespoli[*,1], S. Masuzaki[2,3], K. Tanaka[2,4], M. Shoji[2], R. Lunsford[1], N. Ashikawa[2,3,†], E.P. Gilson[1], N. Tamura[5], D. Medina-Roque[6], T. Kawate[7], T. Oishi[8], K. Ida[2,3], M. Yoshinuma[2,3], Y. Takemura[2,3], T. Kinoshita[4], G. Motojima[2,3], M. Osakabe[2,3], N. Kenmochi[2,3], G. Kawamura[9], T. Singh[10], H. Takahashi[2,3], K. Ogawa [2,3], C. Suzuki[2,3], A. Nagy[1], A. Bortolon[1], N.A. Pablant[1], A. Mollen[11], D.A. Gates[12], T. Morisaki[2,3]

[1] *Princeton Plasma Physics Laboratory, 100 Stellarator Road, Princeton, NJ 08540, United States of America*
[2] *National Institute for Fusion Science, 322-6 Oroshi-cho Toki, Gifu 509-5292, Japan*
[3] *The Graduate University for Advanced Studies, SOKENDAI, 322-6 Oroshi-cho Toki, Gifu 509-5292, Japan*
[4] *Interdisciplinary Graduate School of Engineering Sciences, Kyushu University, Kasuga, Fukuoka, 816-8580, Japan*
[5] *Max-Planck-Institut für Plasmaphysik, 17491 Greifswald, Germany*
[6] *Laboratorio Nacional de Fusión, CIEMAT, Madrid, Spain*
[7] *National Institutes for Quantum Science and Technology, Naka, Ibaraki 311-0193, Japan*
[8] *Department of Quantum Science and Energy Engineering, Tohoku University Sendai, Japan*
[9] *National Institutes for Quantum Science and Technology, Rokkasho, Aomori 039-3212, Japan*
[10] *Department of Mechanical Engineering and Mechanics, Lehigh University, Bethlehem, PA 18015, United States of America*
[11] *Department of Electrical Engineering, Royal Institute of Technology, Stockholm, Sweden*
[12] *Thea Energy, Inc., Kearny, NJ, United States of America*
[†] *Current affiliation: Kyoto Fusioneering Ltd. Distribution A Building, AW1-S, Tokyo Ryutsu Center, 6-1-1 Heiwajima, Ota-ku, Tokyo 143-0006, Japan*
[*] *Corresponding author. Email: fnespoli@pppl.gov*

Abstract

The Impurity Powder Dropper (IPD) is a device capable of injecting controlled amounts of sub-millimetre powder into the plasma under the action of gravity. In 2019 the IPD was first installed on the Large Helical Device (LHD) in Japan, with the aim of improving the plasma performances through real time boronization and assessing the compatibility of this technique with steady state operation. Extensive series of experiments have been performed using the IPD, focused on the improvement of the plasma performance via low-Z powder injection and the understanding of the underlying physical phenomena. In this article, we review the experiments that took place in the period 2019-2024. The main results include the demonstration of the improvement of the wall conditions (reduction of intrinsic impurity content, wall recycling) both on a shot-to-shot basis and in real time. Furthermore, a reduced-turbulence improved confinement regime has been observed coincident with powder injection, resulting in an increase of the plasma temperature of the order of 25%, with enhancements that can reach up to 50% for ion temperature.

1 Introduction

In magnetic confinement fusion reactors, the plasma wall interactions can substantially affect the plasma performances. Early on, wall conditioning techniques have been developed to reduce wall recycling and impurity contamination of the plasma. The need for wall conditioning, already evident for carbon wall machines, is even stronger in the case of metal walls, where the presence of high-Z materials would make the contamination of the plasma more severe even for a much lower impurity concentration, limiting plasma performances or even leading to radiative collapses or disruptions. The wall conditioning technique most widely used worldwide is glow discharge boronization (GDB)

[1]. Despite its beneficial effects on the plasma performance, it presents downsides, namely the use of toxic explosive gases such as diborane B_2H_6, and the need to halt plasma operation to restore wall conditions. This is particularly problematic for future fusion reactors, operating continuously in steady state to produce electricity, and employing superconducting coils, which would need to be turned off during GDB. Recently, an alternative wall conditioning technique which overcomes these limitations has been employed in both tokamaks and stellarators around the world (e.g. ref. [2, 3]): real time wall conditioning via powder injection. Here, boron (B) or B composite powder is injected directly into the plasma where it is evaporated, and the resulting B ions are finally deposited on the plasma facing components.

1.1 The Impurity Powder Dropper

The tool that makes real time boronization via powder injection possible is the Impurity Powder Dropper (IPD). The IPD is designed and built by PPPL, and is capable of delivering controlled amounts of sub-millimeter powder grains to the plasma under the action of gravity [4]. The IPD features four independent feeders units, each one being composed of a powder reservoir and a movable tray that is vibrated at a resonant frequency using piezoelectric actuators. As a result of the vibration, the powder is moved along the tray and eventually falls into the drop tube leading to the plasma. The amount of powder delivered to the plasma can be controlled by adjusting the driving voltage to the piezo actuators, determining the amplitude of the vibration and finally the mass injection rate delivered to the plasma. Each feeder is equipped with an accelerometer, measuring the amplitude of the tray vibration. Furthermore, a flowmeter monitors the amount of powder dropped into the tube: here, a horizontal collimated beam of light crosses the falling powder stream; a photo diode measures the light transmitted to the other end of the powder stream, measuring the attenuation resulting from the powder falling through it. For each powder type, calibrations are performed in laboratory settings or in-situ, providing calibration curves of the delivered mass rates as a function of both the accelerometer signal amplitude and the attenuation of the flowmeter signal, allowing an estimation of the amount of powder delivered to the plasma during the experiments. A schematic of the IPD is shown in Fig. 1. The presence of four separate feeder units allows the use of up to four different powder types (size, material) during the same experimental run.
Prior to the installation of an IPD on LHD, similar devices was already operative on several tokamaks, such as DIII-D [2], ASDEX Upgrade [5], EAST [6] and KSTAR [7]. Shortly after the installation on LHD, an IPD was installed on the WEST tokamak as well [8]. Encouraged by the LHD results reviewed in this paper, as well as result from powder injection experiments in W7-X using a smaller device, the Probe Mounted Powder Injector [3, 9], the installation of an IPD is currently ongoing on W7-X [10]. Finally, due to the growing importance of wall conditioning following the decision to move to a full tungsten wall, the implementation of a similar device has been proposed for ITER as well [11].

1.2 Installation on LHD and first experiments

In 2019, the IPD was first installed on the Large Helical Device (LHD) in Japan. The primary aim was to assess the compatibility of real time wall conditioning with steady state operation, as LHD can sustain plasmas with durations up to one hour [12, 13]. The installation of the IPD on LHD was guided by coupled EMC3-EIRENE and DUSTT simulations [14, 15], to maximize the penetration of the powder grains into the LHD plasma. Indeed, LHD has a unique magnetic configuration, featuring a helically rotating double-null like divertor connected to the main plasma by a thick ergodic layer. Simulations were performed coupling the EMC3-EIRENE code [16, 17]

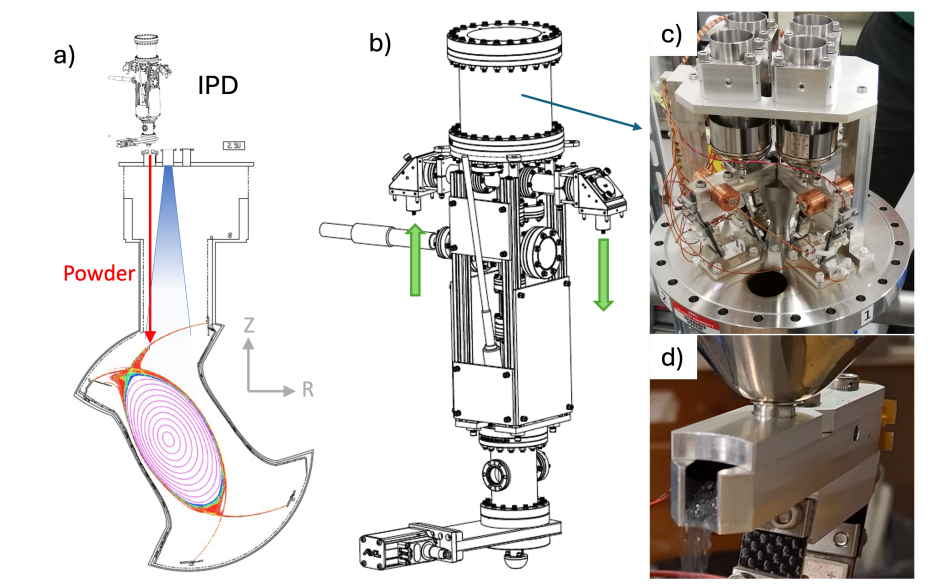

Figure 1: a) position of the IPD on the LHD vacuum vessel and relative plasma cross section. b) Schematics of the IPD highlighting the flowmeter (green arrows) and the position of the c) powder reservoirs and the piezoelectric vibration stage. d) Boron powder flowing from the feeder into the drop tube.

describing the stellarator plasma edge, and the DUSTT code [18], which solves for the trajectories of powder grains injected into the plasma. Simulations of powder injection were performed for four different ports available for the installation of the IPD. Indeed, the powder grains have to cross the divertor leg in order to reach the main plasma, and they can be deflected by the ion drag force associated with the plasma flow in this region. The deflection of the powder grains can be more or less effective depending on the plasma parameters, the powder grain material and size, and geometrical factors such as the relative position of the injection location with respect to the plasma equilibrium. An example of the resulting powder trajectories is shown in Fig. 2. The port maximizing the penetration of the powder into the ergodic layer was chosen for the installation of the IPD.

The final position of the impurity powder dropper on LHD is shown in Fig. 1a, together with the field of view of a visible camera monitoring the powder injection into the plasma (in blue in the figure).

A first set of experiments was performed injecting both boron (B) and boron nitride (BN) powder into 4 second long plasma discharges. The nominal size of the powder grains was 150 μm for B and 60 μm for BN. Visible camera imaging, UV and charge exchange spectroscopy confirmed the successful injection of the powders into the plasma, for two different magnetic configurations, namely at $R_{ax} = 3.6$ m and $R_{ax} = 3.9$ m [19]. Visible camera images of B and BN powder entering the plasma are shown in Fig. 3, together with images of the injection of different powder materials which were performed in later experiments. The plasma response to the powder injection was characterized by systematically scanning the plasma density and powder injection rates. As a result, the relative perturbation on plasma density due to powder injection decreases for higher densities and lower injection rates. The radiated power increases with the injected mass rates, especially for BN powder. Spectroscopic measurements of UV B lines [20] as well as form Charge Exchange Recombination Spectroscopy (CXRS) show a deeper penetration of the powder grains

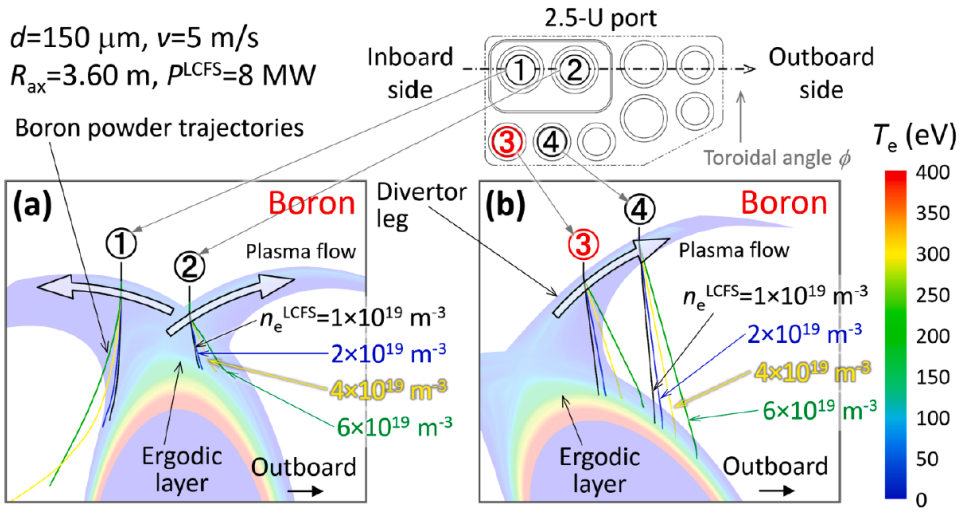

Figure 2: Results of powder grains trajectories from coupled EMC3-EIRENE and DUSTT simulations for boron powder grains for different port locations and different plasma densities. Reprinted from [M.Shoji et al., Nucl. Mater. and Energy 41, p.101803 (2024)] [15] under CC-NC-ND license.

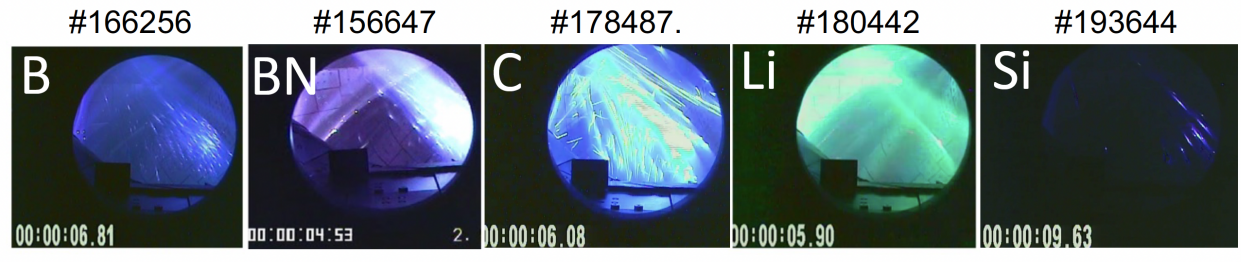

Figure 3: Visible camera images of powder entering the plasma, for different powders materials. From left to right: boron, boron nitride, carbon, lithium, silicon.

into the plasma for low plasma densities, in line with previous simulation results [14], since the plasma flow in the divertor leg is less effective in deflecting the powder trajectory from the vertical direction at low plasma densities. Furthermore, the spectroscopic measurements showed how the B ions were expelled more efficiently for the low density plasma, consistently with the outwards direction of the radial electric field for those electron-root regime plasmas. This, together with simulation results showing how the injected boron atoms are more uniformly deposited on the wall at low plasma densities [21], suggests that low density plasmas might be a better candidate for real time wall conditioning applications.

2 Wall conditioning experiments

Wall conditioning techniques have been developed early on in fusion machine to better control the influx of both impurities and gas fuel from the plasma facing components (PFCs). Wall conditioning techniques are being employed routinely in tokamaks and stellarators around the world to access lower collisionality plasmas. While many wall conditioning schemes are available, the most popular

ones employ deposition of layers of low-Z materials on the PFCs. Several material choices have been explored in the past, using materials such as C and Si, and Li which is currently used regularly by several devices, most notably the EAST tokamak. Nevertheless, the most widely use wall conditioning technique is the glow discharge boronization (GDB). Here, a plasma glow discharge is performed using diborane gas (B_2H_6). The B atoms resulting from the ionization of the gas are deposited on the PFCs creating a thin film. As the glow discharge boronization is performed in absence of magnetic field, the film is deposited evenly across the wall, even in regions that are not directly touched by the plasma. Future fusion reactors are envisioned to operate quasi-continuously in steady state conditions, for hours at a time, with high-Z metallic walls. In this situation, wall conditioning gains even more importance, and additional or alternative wall conditioning techniques are needed for a safe operation of the reactor. Indeed, the glow discharge boronization requires the magnetic field to be turned off, interrupting plasma operation. This is an issue for reactors employing superconducting coils, as ramping down and up again the magnetic field can be quite time consuming. Furthermore, the thin B layer deposited during the glow discharge is projected to wear off in less than one hour, as the high plasma fluxes at the contact points would erode it. A solution to this problem could be provided by real time boronization. Here, B powder is injected and evaporated into the plasma, and B ions are finally deposited on the wall. Wall conditions can be replenished without the need to halt plasma operation. Furthermore, with this technique B would be preferentially deposited in the regions of the PFCs directly touched by the plasma, where the original B layer would have been eroded faster.

2.1 Boronization via powder injection

The wall conditioning effects of injecting boron powder into the plasma have been investigated with series of dedicated experiments, and are reported in Ref. [22]. First, the effects of cumulative powder injection have been evaluated comparing two identical density ramp discharges performed before and after injection of B and BN powder into the plasma, for a total amount of approximately 2 g B introduced into the plasma. As a result, the content of intrinsic impurities was reduced by the cumulative powder injection: oxygen level is decreased by a factor of 3, and carbon level is reduced up to a factor of two, as shown in Fig. 4a,b. This is consistent with gettering and codeposition of the O and C impurities with a newly deposited B layer on the plasma facing components (PFCs). This result was obtained just after a vacuum vessel vent, before a standard GDB. The repetition of the experiment after a GDB, where 37g B are deposited on the PFCs, resulted in a smaller decrease of intrinsic impurities resulting from cumulative powder injection of 1g B. Nevertheless, comparing two otherwise identical discharges before and after the cumulative powder injection, the resulting plasma density is 18% lower after powder injection (Fig. 4c). This can be interpreted as a reduction of recycling due to the deposition of B atoms on the wall. A similar reduction of density was observed as well for the discharges compared in Fig. 4a,b even though the comparison is made more difficult by a non-identical gas puff for the two discharges (unlike in Fig. 4c), and by the failure of one of the NB heating sources in discharge #156166. Nevertheless, during the phases with comparable heating $t < 4.165\ s$, the discharge after cumulative B injection (#156166) reached a 13% lower plasma density with respect to the reference discharge (#156149), despite an overall slightly higher gas puff source. The deposition of a thin film of boron on the PFCs is confirmed by the post-mortem optical emission spectroscopy analysis of a material sample located on the LHD first wall, which has been exposed to the IPD experiments [23]. Spatially resolved spectroscopic measurements of emission from BH molecules and B^+ ions confirmed these species are concentrated in the divertor region during powder injection, suggesting B ions are deposited on the divertor as well [24]. The spectroscopic investigation also showed the decrease of neutral hydrogen in the scrape

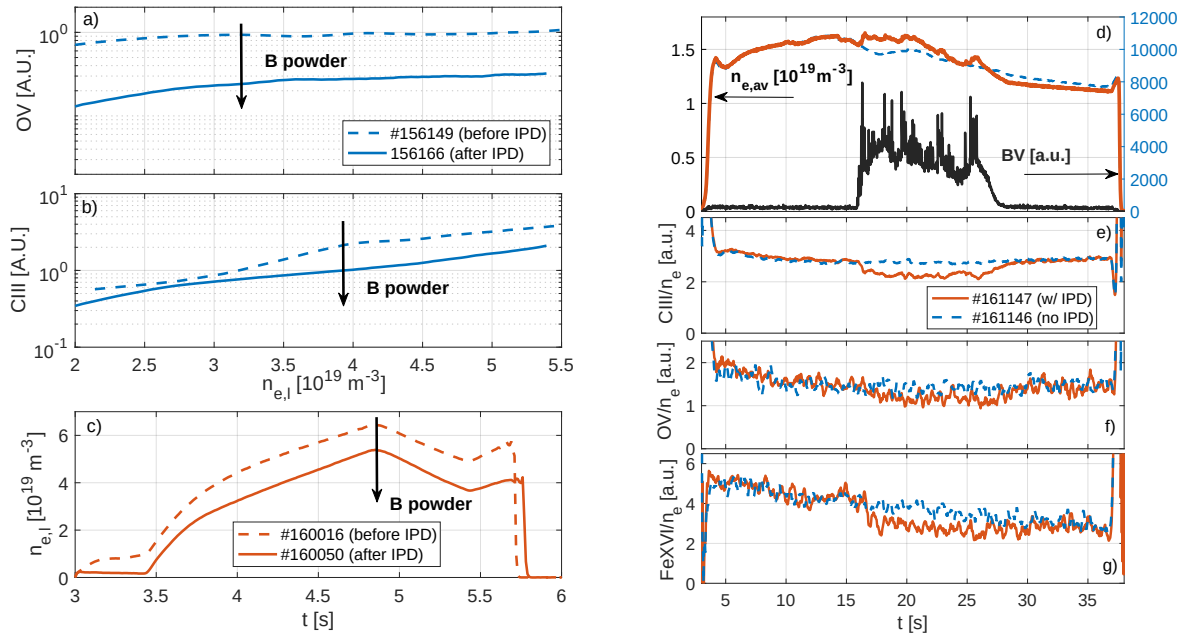

Figure 4: UV spectroscopy OV (a) and CIII (b) lines during density ramp up before (dashed) and after (solid) cumulative B powder injection, plotted against line averaged density. c) Line averaged density of discharges with same gas puff, before (dashed) and after (solid) cumulative B powder injection. d) Density evolution during B powder injection (solid) compared with a reference discharge (dashed), together with evolution of BV UV spectroscopy measurement. e-g) Evolution of UV spectroscopy lines of intrinsic impurities.

off layer region during powder injection, confirming the decrease of wall recycling.

2.2 Real time boronization

In a second series of experiments where real time wall conditioning was investigated [22], B powder is injected for 10 seconds in a 40 s long hydrogen (H) plasma discharge, and compared with an otherwise identical reference discharge, as is shown in Fig.4 d-g. In particular, in both discharges, for $t < 15$ s the H gas puff is controlled via feedback to keep the average density to a prescribed level; for $t > 15$ s, to better evaluate the wall conditioning effects of B powder injection, the H gas puff is set to zero, making recycling/outgassing from the PFCs the only H source in this phase. As a result of B injection, performed in the phase without H gas puff, the line averaged electron density is at first increased by the additional electron source provided by the powder, but after a few seconds it recovers the reference level, and remains lower than the reference value after the end of the powder injection. This can be interpreted as a real time reduction of recycling given by the deposition of B atoms on the wall. Simultaneously, the level of intrinsic impurities (C, O, Fe) is decreased during the powder injection, recovering the reference level after the powder injection is stopped. This could be the results of a change in transport induced by B injection, rather than a decrease of the influx of intrinsic impurities from the PFCs due to the real time deposition of a B layer. Similar real time wall conditioning effects have also been observed during B powder injection into helium plasmas, where the reduction of recycling, even in absence of chemical bonding between boron and He, suggests this reduction could be caused by co-deposition [25].

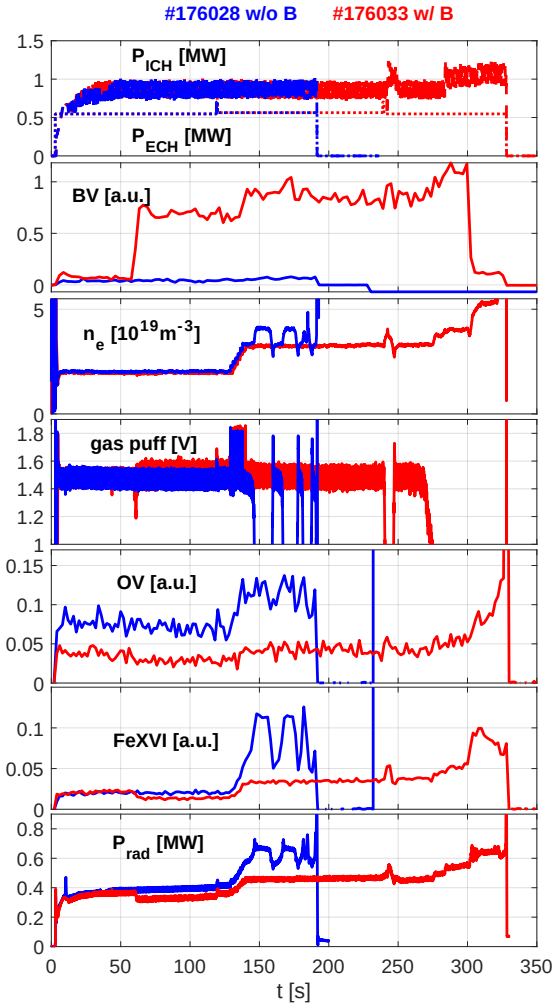

Figure 5: Time traces of (from top to bottom): input ECH (dotted) and ICH (solid) power, BV line from EUV spectroscopy, line averaged density, gas puff, OV line from EUV spectroscopy, FeXVI line from EUV spectroscopy, and total radiated power from bolometry. A discharge with B powder injection (red) is compared to a reference discharge (blue).

2.3 Application to long plasma discharges

Leveraging the real time wall conditioning capabilities of the IPD demonstrated in Ref. [22] and reported in the previous subsection, boron powder injection was used in minutes-long hydrogen discharge to provide real time wall conditioning, improving density control and eventually extending the discharge duration by avoiding an otherwise occurring radiative collapse [26]. In this experiment, B powder was dropped continuously for 240 seconds in a 5 minutes-long plasma, as shown in Fig. 5. In a reference discharge without powder injection, following a controlled increase of density at about $t \sim 130$ s, density control is lost as density increases even if the gas puff fueling is set to zero. The total radiated power is increased, together with the radiation lines OV and FeXVI from UV spectroscopy measurements, taken as a proxy for the concentration of the O and Fe intrinsic impurities. Due to cumulative injection of B powder in subsequent shots, the oxygen level is decreased since the beginning of the discharge. With the beginning of powder injection, the gas puff required to sustain the same plasma density is increased, suggesting the recycling of H at the

wall is reduced. At the same time, the Fe level is also reduced with respect to the reference discharge, suggesting a change in impurity transport. The total radiated power, measured by bolometry, is reduced in a similar fashion. When the programmed density increase is reached, density control is not lost, O and Fe concentration are kept approximately constant and the total radiated power is increased only proportionally to the density. As a result, the uncontrolled density increase at $t \sim 190$ s and consequent plasma collapse are avoided, showcasing a successful demonstration of the real time wall conditioning technique.

2.4 Wall conditioning with different powder materials

While boronization is the most widely used wall conditioning technique, other low Z materials can be used as well to achieve the same effect. In particular, Li is routinely used in the EAST tokamak for wall conditioning purposes, as well as in smaller machines such as HIDRA and LTX-β. Wall conditioning with other materials was attempted in the past as well, such as carbonization and siliconization. While Si has higher Z than B and is potentially more polluting for the plasma, Si offers potential advantages as a surface material, like lower sputtering rates and reduced hydrogen retention, as well as longer lasting conditioning effects. Siliconization was compared to boronization in ASDEX-Upgrade [27] and EAST [28], and was found to have similar or even better wall conditioning properties. Recently, interest is growing to consider silicon carbide (SiC) as a candidate for plasma facing components material [29, 30]. A first series of experiments was recently performed in LHD to investigate the use of silicon powder injection for real time wall conditioning. Similarly to what was done for B powder (see Fig. 4d-g), Si powder was injected for 10-20 seconds into 6 40 second long plasmas heated by 0.6 MW ECH. The plasma density is controlled by a feedback mechanism on the gas puff fueling. The results of the experiment are shown in Fig. 6. The injection of the powder into the plasma results into a remarkable increase of radiated power, up to 80%, with respect to the reference discharge (in black in the figure). No visible effect on the plasma density nor the gas puff is observed during or after powder injection, suggesting that the wall recycling is not altered. While a shot-to-shot variation of the OV and FeXVI UV spectroscopy line is observed, no clear trend of reduction or increase of those impurities concentration can be deduced. On the other hand, a clear reduction of CIII radiation can be observed, especially during the time window of the powder injection itself. Once again, this might be induced by a change in plasma impurity transport rather than wall conditions. The different response for different intrinsic impurities (C, O, Fe) might be due to a dependence on impurity charge of the fluxes, and/or to the different location of the sources (divertor/first wall). Further analysis to disentangle those effects will be needed, and are reserved for future works.
The lack of clear wall conditioning effects might be due to the fact that these low density, low power plasmas can sustain only a limited amount of Si powder, which is both higher Z and a more effective radiator than B, without collapsing. The low amount of powder grains entering the plasma during this experiment can be appreciated in Fig. 3. Therefore, the amount of Si powder introduced in this series of experiments might not be sufficient to deposit enough Si on the wall to start to observe wall conditioning effects. Repeating these experiments with higher density and higher power plasmas, thus able to assimilate more Si powder, might lead to the observation of clearer wall conditioning effects.

Finally, the wall conditioning effects of lithium powder injection were investigated in a dedicated series of experiments. The results are currently being analyzed and will be detailed in future publications.

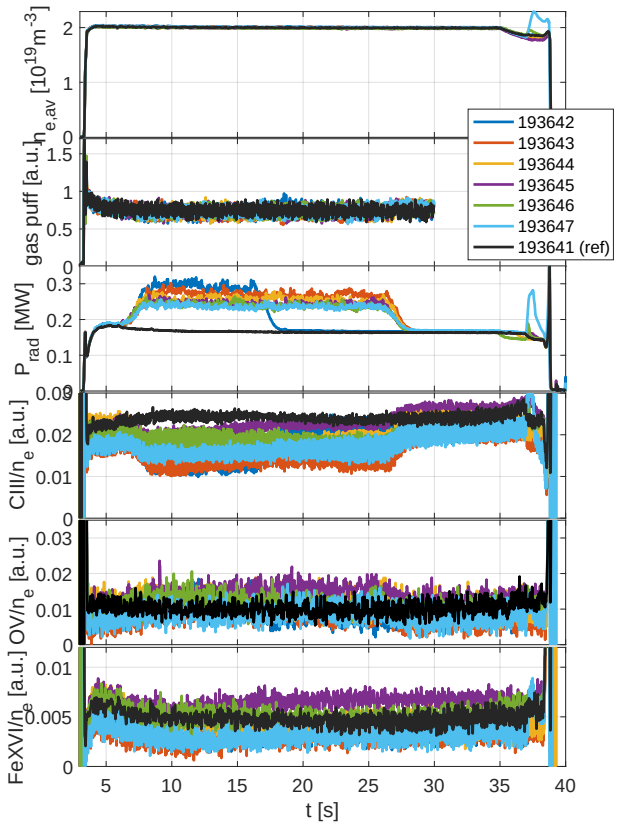

Figure 6: Time traces for consecutive shots with Si powder injection of (from top to bottom): line averaged density, gas puff, total radiated power, CIII, OV and FeXVI UV lines normalized to density. The reference discharge, first of the series and with no powder injected, is plotted in black.

3 Performance improvement via powder injection

3.1 Access to a reduced turbulence, improved confinement regime via boron powder injection

The injection of B powder into the plasma has been observed to cause an improvement of the plasma performance, with a marked increase of both plasma temperature (electron and ion), stored energy and confinement time [31]. At the same time, the turbulent density fluctuations measured by phase contrast imaging (PCI) diagnostic have been observed to decrease by up to a factor of 2 in a wide portion of the plasma volume. In matched discharges with the same input power and line averaged density, kept constant by a feedback control, the increase of plasma temperature upon B powder injection is of the order of 25%, but the ion temperature can increase by up to almost 50% upon powder injection under certain conditions. Typical increases of stored energy W_p and energy confinement time τ_E are of the order of 15%. The transition to this reduced turbulence, improved confinement regime has been observed for different heating schemes (ECH, NB, ECH+NB+ICH), for both H and D main plasma ions and for both directions of the magnetic field. Two examples are shown for a deuterium and an hydrogen plasma respectively in Fig. 7, discharge #166256 (subplots a,b,c,g), which has been analyzed in details in Ref. [31], and discharge #167234 (subplots d,e,f,h).

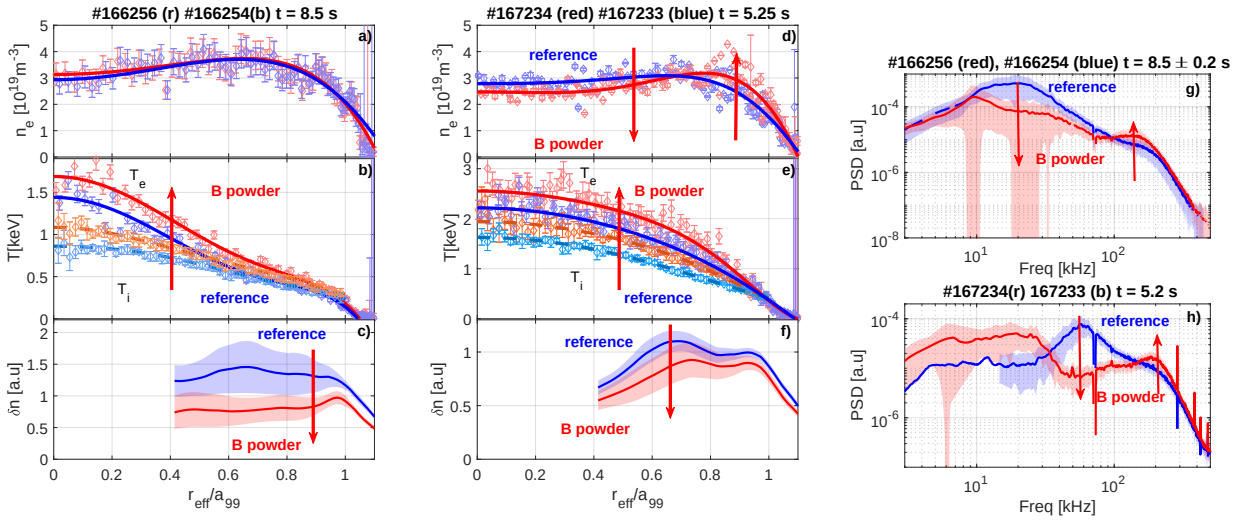

Figure 7: Radial profiles of a,d) electron density b,e) electron (solid) and ion (dashed) temperature c,f) turbulent density fluctuations. g,h) Turbulent fluctuation spectrum. Red: boron powder injection discharge. Blue: reference discharge. Two different examples are shown (a,b,c,g and d,e,f,h)

Here, radial profiles for a boron powder injection discharge are shown in red and compared with an identical reference discharge without powder in blue. As a result of powder injection, the density profile generally becomes more peaked in the edge and hollower in the center (even though this effect is small for the discharge #166256). This can be due to the extra electron source provided by the powder, which is evaporated just outside the last closed flux surface according to EMC3-EIRENE simulations coupled with the DUSTT and DIS codes. Also, the increase in electron temperature can contribute to the hollowing of the profile increasing the neoclassical particle flux. For the discharge in Fig. 7, H_α radiation from neutral hydrogen is observed to decreased during powder injection, as well as plasma density in the divertor, suggesting a decrease in recycling during boron injection. This effect might contribute to steepening the electron density profile at the edge of the plasma. Intrinsic impurity concentration (C, Fe) is also observed to decrease during B powder injection, similarly to what was already reported during wall conditioning experiments detailed in section 2. At the same time, temperature profiles are steepened in the edge, increasing T_e and T_i over the whole cross section. At the same time, the turbulent density fluctuations Fig. 7c are decreased in most of the plasma cross section (no PCI measurement is available for $r_{eff}/a_{99} < 0.4$).

3.2 Further experiments with different plasma conditions, powder materials

To better characterize the improvement upon powder injection, and to understand the underlying physical phenomena, an extended series of experiments has been performed, where the plasma density, input power, injection mass rate have been scanned systematically, and different powder materials have been compared [32]. As a result, the relative ion temperature increase $\Delta T_i/T_i$ is observed to increase with the amount of injected powder for each plasma scenario considered (plasma density, heating power/scheme). If the injection mass rate exceeds a certain threshold, the value of which depends on the plasma scenario, density control can be lost leading to increase to the plasma density, and even plasma collapse. While generally always remaining positive, $\Delta T_i/T_i$ is reported to decrease with both electron density and input power. Across this extensive database, no clear trend could be established for the turbulence response. The modification of turbulence upon powder

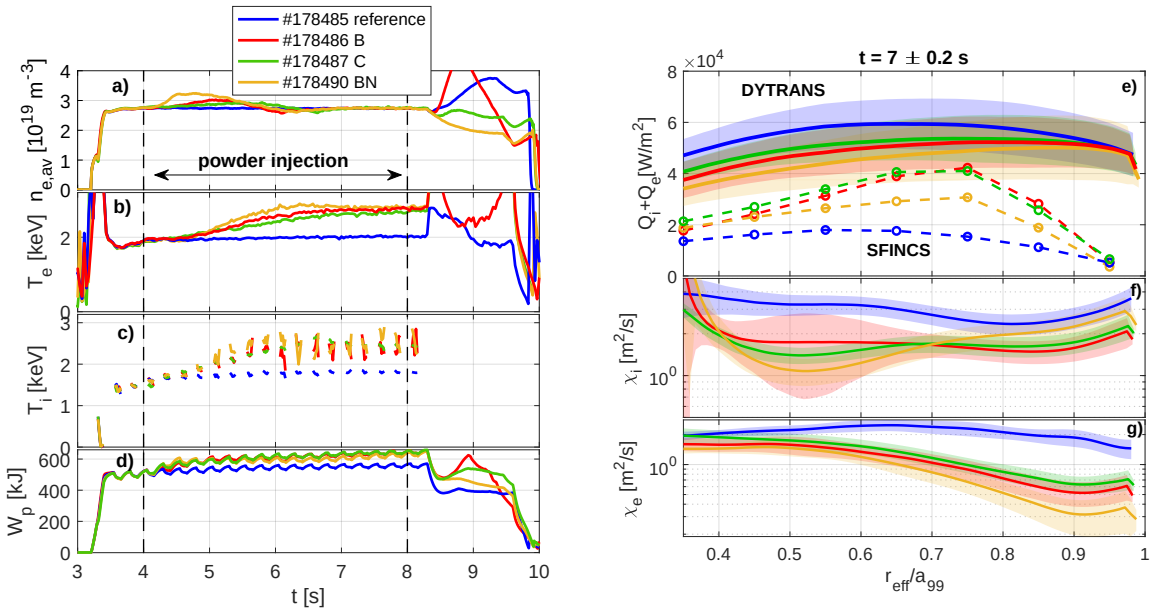

Figure 8: Comparison of the effect of different powders: B (red), C (green), BN (yellow) with respect to reference discharge (blue). Time traces of a) electron density b) electron temperature c) ion temperature d) stored energy. Powder injection time window is marked by vertical dashed lines. Radial profiles e) of total heat flux from DYTRANS analysis (solid), neoclassical heat flux from SFINCS simulations (dashed) f) ion and g) electron thermal conductivities from DYTRANS.

injection is found to depend on the initial state of the plasma and its turbulence type/level, and any case should be analyzed in detail. The access to the reduced turbulence, increased confinement regime has been observed for different powder materials, namely B, BN and C. The time traces of an experiment comparing the three powder materials are shown in Fig. 8. Here, the powder is injected into the plasma starting at approximately $t = 4$ s, until $t = 8$ s. Initially, the electron density is increased $\sim 10\%$ above the reference level due to the extra electron source provided by the powders, and is then recovered by the feedback on the gas puff within 2 s. After this transient phase, for the three materials, a similar increase of temperature $\sim 30\%$ has been reported for both ions and electrons. The plasma stored energy W_p also increases similarly for the three different powder types. The turbulence response was similar as well for the three different powders, with decrease of turbulent fluctuations inside the LCFS and for lower frequencies, while higher frequency modes are excited, in a similar manner to the case discussed beforehand in Fig. 7. In all cases, dynamic transport analysis with the DYTRANS code [33, 34] reveals a substantial decrease of thermal diffusivities in the region $0.4 < r_{eff}/a_{99} < 0.9$, up to 50% for the ions and up to 2/3 for electrons, as shown in Fig. 8f,g. Intrinsic impurity concentration is observed to generally decrease for the three different powder materials. After a few seconds of powder injection, the H_α radiation recovers the reference level after an initial decrease, while the gas puff is increased to maintain a constant line averaged density, suggesting a decrease of wall recycling. This similar behavior occurs for the three powder materials (even C), so that wall conditioning effects can not be excluded from the possible cause of accessing the improved confinement regime. Turbulence reduction has been observed also upon Li powder injection, as will be detailed in subsection 3.4. However, a direct comparison of the effect on turbulence of B and Li powder is missing up to this day. This comparison was attempted in a dedicated experiment where big Li powder grains ~ 850 μm were used to improve penetration of the light Li powder into the plasma. However, the density perturbation introduced

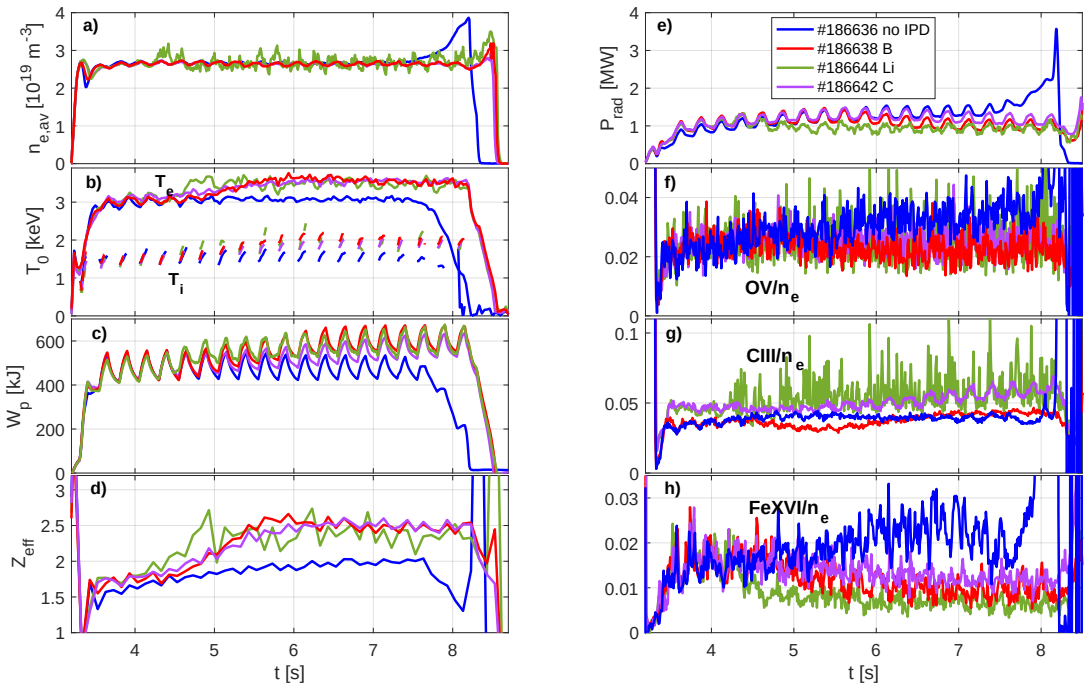

Figure 9: Comparison of different powder materials: B (red), C (purple) and Li (green) compared with a reference discharge (blue). Time traces of a) electron density b) ion and electron temperature c) stored energy d) plasma effective charge e) total radiated power, spectroscopic measurement of line radiation normalized to electron density of the OV (f) CII (g) and FeXVI (h) lines.

by the evaporation of the single granules were not negligible on the plasma with a relatively low density $n_e \sim 2.5 \cdot 10^{19} m^{-3}$, compromising the turbulence measurements. In this experiment, the injection mass rate of the B, C and Li powders was scanned on a shot to shot basis. Discharges with similar values of $Z_{eff} \sim 2.5$, supposedly one of the controlling parameters for turbulence reduction and confinement improvement, are selected a posteriori for a more meaningful comparison of the effects of the different powder materials (for comparison in the reference discharge $Z_{eff} \sim 2$). The results of this comparison are shown in Fig. 9. Despite the above mentioned non-conclusiveness of the turbulence measurements for the Li case, a similar increase of both T_i, T_e and W_p was observed for the three powder materials, being $\Delta T_i/T_i = (30\%,\ 24\%,\ 21\%)$, $\Delta T_e/T_e = (18\%,\ 14\%,\ 15\%)$, $\Delta W_p/W_p = (25\%,\ 21\%,\ 13\%)$ for B, Li, C respectively. Those values are computed as an average over the time window $6 \leq t[s] \leq 7$. Over the same time window, the energy confinement time is increased $\Delta\tau_E/\tau_E = (21\%,\ 19\%,\ 12\%)$ for B, Li, C. B and Li powder resulted in similar reduction of radiated power $\Delta P_{rad}/P_{rad} = (-20\%,\ -30\%)$ respectively. A slight reduction in P_{rad} is observed for C powder as well $\Delta P_{rad}/P_{rad} = -6\%$. This might be due to the fact that the three different powders appear to be effective in the reduction of intrinsic impurities such as O and Fe. The smaller reduction in radiated power in the case of C powder is consistent with the introduction of a more effectively radiating impurity with respect to B and Li, and might explain a lesser increase in performances for C.

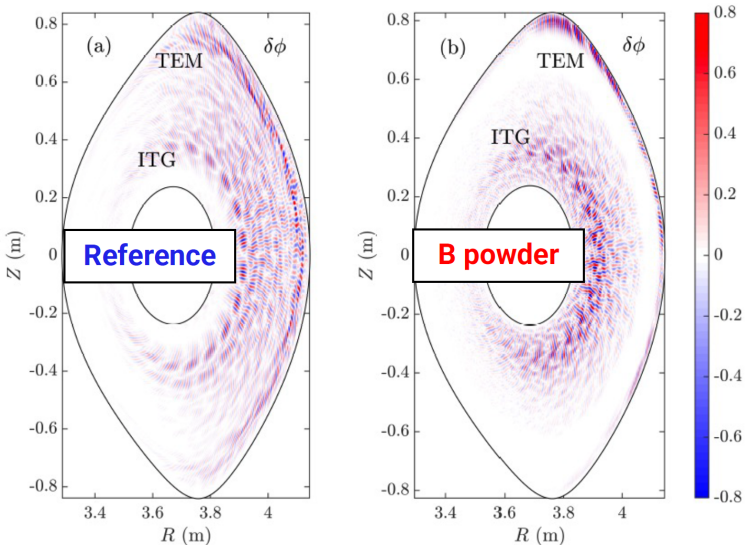

Figure 10: Distribution of the potential fluctuations for the linear phase of global gyrokinetic simulations with the GTC code in the case without (a) and with boron (b). Modified and reprinted from [T. Singh et al., Nucl. Fusion 64 (2024) 016007] [36] under CC-BY 4.0 license.

3.3 Interpretation

The increase of T_e, T_i and W_p with powder injection is associated with a reduction in energy transport in the edge of the plasma. Indeed, in Ref. [31] transport analysis performed with the DYTRANS module of TASK3D-a has shown that the thermal conductivities for electrons and ions χ_e and χ_i are reduced by more than 40% in the edge of the plasma $r_{eff}/a_{99} > 0.4$. This result is consistent with a decrease of turbulent transport, as SFINCS [35] simulations have shown that during powder injection both the main ion particle and neoclassical heat fluxes are increased. Since the input power is the same with/without powder, and the discharges are in steady state, the total heat flux computed by DYTRANS is approximately the same in the case with and without powder. By difference, the increase in neoclassical transport implies then a reduction in the turbulent component of the transport. The same analysis has been repeated in Ref. [32] for the case comparing different powder materials, finding similar results, shown in Fig. 8e-g. Furthermore, the SFINCS simulations in Refs. [31, 32] show how the injection of powders produces only minor changes in the ambipolar radial electric field E_r, suggesting a more negative E_r or the increase in E_r shear could be excluded as mechanisms for turbulence stabilization in this case.

For discharge #166256, analyzed in detail in Ref. [31], the analysis of the PCI turbulent spectrum resolved in terms of wavenumber reveals turbulence peaking for $k_\perp \sim 0.3$ mm^{-1} before powder injection, which in previous LHD analysis had been found to be consistent with ITG turbulence [37]. During powder injection, this peak is substantially decreased. This lower frequency turbulence is decreased (peak around 20 kHz in Fig. 7d, showing the turbulent spectrum in terms of frequency), while higher frequency fluctuations are increased. This might be due to a destabilization of TEMs in the edge of the plasma where density and its gradient are increased. Dedicated global gyrokinetic simulations of discharge #166256 (Fig. 7) have confirmed the presence of both ITG and TEM turbulence, as detailed in Ref. [36]. The distribution of the potential fluctuations for the linear phase of the simulations in the case without and with boron is shown in Fig. 10. The numerical simulations were able to reproduce the mode frequency, estimated to be $\sim$ 20 kHz for ITGs and $\sim$ 80 kHz for TEMs. For the case featuring boron, the frequencies are shifted to $\sim$ 13 kHz for ITG

and $\sim$ 100 kHz for TEMs, which is judged to be consistent with the experiments (Fig. 7d). The effective thermal diffusivity χ_{eff} was found to be in good quantitative agreement with the experimental values resulting from a DYTRANS analysis. Nevertheless, the decrease in transport upon addition of B ions was not well captured by the simulations. One possible explanation could be the lack of EM effects in the simulations. Indeed, recent experiments suggest that resistive interchange turbulence might be important in the edge of LHD plasma [38].
Furthermore, as mentioned in the previous subsection and detailed in Ref. [32], more in general the turbulence response to powder injection varies with the plasma scenario (density, heating power/source). Indeed, the different scenarios exhibit different PCI spectra, suggesting different turbulence types might be dominating transport in the different scenarios. Consequently, turbulence response varies from case to case and drawing a general picture is not possible at this point, and each case should be analyzed in detail. For example, for discharge #174829 analyzed in detail in Ref. [39], the main peak in the turbulence spectrum at $\sim$ 60 kHz is judged to be consistent with TEM turbulence rather than ITG. This peak is substantially suppressed by powder injection, suggesting reduction of TEM turbulence in the plasma core. But as detailed in Ref. [32], the turbulence level can even increase upon powder injection, for low plasma density cases. Recent theoretical investigations have shown how impurity concentration can strongly affect stellarator turbulence, both reducing or enhancing it depending on impurity concentration and gradient sign [40]. While each case must be considered singularly, and this phenomena is not fully understood yet, most possibly the improvement of confinement is due to suppression of ion-scale turbulence (either ITG or TEM), due to either the modifications in Z_{eff} and the plasma profiles caused by the powder injection, or both.

3.4 Impurity transport during turbulence suppressed phase

The transport of mid and high-Z impurities during the reduced-turbulence, increased confinement regime via powder injection has been recently investigated in a series of dedicated experiments, which results are detailed in Ref. [41]. Here, mid and high-Z impurities (Ti, Mo) are injected into the LHD plasma using the Tracer Encapsulated Solid Pellet (TESPEL). The characteristic timescale of the decay of extreme UV spectroscopy lines is used as a proxy for impurity confinement time. TESPEL is injected in discharges where continuous Li powder injection is used as a tool to reduce turbulence, and results are compared to TESPEL injections in reference discharges without powder injection. Here, Li powder of approximate size 500 μm is injected in plasmas of density $n_e \sim 5.25 \cdot 10^{19} m^{-3}$ heated by 7 MW NBI. Unlike what was observed in the Li injection experiments described in section 3.2, here turbulence reduction is observed across the portion of the plasma cross section measured by PCI in the region $r_{eff}/a_{99} > 0.4$, with turbulent density fluctuation amplitude being decreased by approximately a factor of 2 during Li powder injection. Electron temperature is increased on average by $\sim$ 12% while T_i on average stays approximately the same. The smaller powder granules and higher plasma density led to relatively weaker density perturbation given by the evaporation of the single Li granules with respect to the results discussed in section 3.2, confirming that the access to the reduced turbulence improved confinement regime is possible with Li powder as well.
The spectroscopic measurements of the TiXX and MoXXXII lines show a faster decay in the case where the TESPEL is injected in the reduced turbulence plasma with Li powder. This suggests that in these LHD plasmas, the transport of heavy impurities is not dominated by turbulence but by neoclassical transport instead. Dedicated SFINCS simulations for those discharges with Mo TESPEL injection show how the ambipolar radial electric field E_r is negative everywhere, consistently with poloidal flow measurements from PCI, and E_r is not noticeably changed during

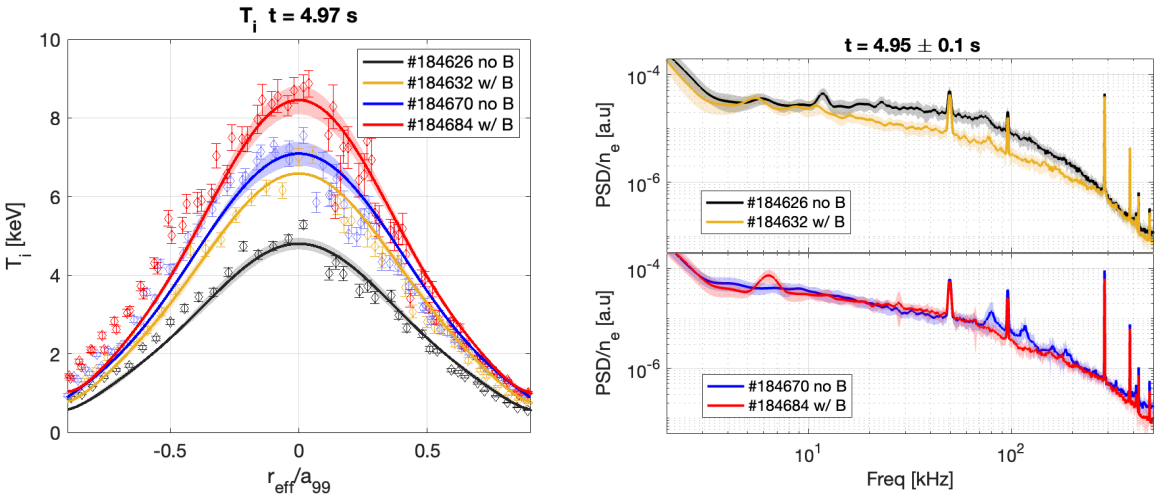

Figure 11: Left: radial profiles of ion temperature measured by CXRS for a case before ICHWC (black: no B, and yellow: with B) and after ICHWC (blue: no B, red: with B). Right: turbulence spectra from PCI normalized to electron density for the same discharges.

the Li powder injection with respect to the reference discharge. While one would then expect an inwards flow of the Mo^{31+} ions driven by E_r, the simulations show how due to the high collisionality for this species in the edge of the plasma, its transport is dominated by the classical contribution rather than the neoclassical one. The classical particle flux, already directed outwards in the reference discharge, is increased even further during Li powder injection, consistently with the spectroscopic measurements. Theoretical studies have indicated that the classical transport could indeed be important for strongly collisional plasma species [42], and our observations point in this direction.

While more analysis is required, this mechanism could potentially explain the reduction of intrinsic impurity transport observed during B powder injection as well, for example in the discharges in figure 4d-g or Fig. 9f-h.

3.5 Application to high ion temperature scenario

In LHD, a "high-T_i" scenario was developed with the aim of maximizing the ion temperature, with the formation of an internal transport barrier (i-ITB), resulting in ion temperatures in the order of $T_i \sim 10$ keV. The scenario consists in high power NBI-heated low density plasmas, where the injection of carbon pellets can help sustain the i-ITB, and wall conditioning methods such as Ion Cyclotron Heating Wall Conditioning (ICHWC) can help achieve low wall fueling for better density control providing access to low collisionalities. A more comprehensive description of the LHD high-T_i scenario can be found in Ref. [43]. As described in Ref. [43], boron powder injection was investigated as a mean to improve the performance of this scenario, both through real-time and cumulative wall conditioning effects due to the powder injection, and as a means of reducing turbulence and further enhancing T_i, leveraging the results detailed in subsections 3.1, 3.2. As a result, continuous B powder injection resulted in an increase of T_i of $\sim 50\%$, reaching $T_i \sim 4.5$ keV, as reported in [43] for discharge #177950. While wall conditioning effects of B powder injection certainly contribute to this result, for this discharge PCI measurements show a reduction of density turbulent fluctuation level for frequencies $F \leq 80$ kHz, consistently with previous observations of turbulence reduction upon powder injection, especially considering higher ion temperature gains

reported for low density, high power plasmas upon B powder injection in Ref. [32].
A further series of experiments have been performed to investigate the effect of B powder injection on this scenario, and the results are shown in Fig. 11. First, boron powder is added to a reference shot where approximately 15 MW NBI are injected into an $n_e \sim 1.3 \cdot 10^{19} m^{-3}$ plasma, in which also one carbon pellet is injected. As a result, ion temperature is increased of about 37% from 4.8 keV to 6.6 keV, as shown in Fig. 11 in black and yellow for the reference discharge and the one with B powder respectively. For this case, turbulence level is clearly reduced on most of the spectrum measured by PCI $F \leq 250$ kHz. In figure 11, the PCI spectrum normalized to the electron density is shown, to account for the $\sim 17\%$ decrease in n_e due to the introduction of B powder.
Then, ion cyclotron heating (ICH) wall conditioning is performed. As a result, temperature is increased further to $T_i \sim 7$ keV (without B powder injection). Though, the density is decreased down to $n_e \sim 0.8 \cdot 10^{19} m^{-3}$ as an effect of the wall conditioning, so that overall the effect of ICH wall conditioning and B powder injection appears comparable, as already noted in Ref. [43]. The injection of B powder after the ICH wall conditioning results in a further 20% increase in $T_i \sim 8.45$ keV. Here, boron powder resulted in an increase of electron density of $\sim 19\%$ with respect to the reference discharge. The normalized turbulent density fluctuation spectrum, shown in blue and red in Fig. 11 respectively, is slightly decreased only in the higher frequency part of the spectrum $F \geq 80$ kHz. While dedicated modeling efforts would be needed for the correct interpretation of these results, these experiments constitute a successful demonstration of B powder injection as a tool to reduce turbulence and improve performances for already high-performance plasmas.

4 Other experiments

4.1 Effect of powder injection on density limit

In a fusion reactor, the produced fusion power scales with the density as $P_{fus} \propto n^2$, therefore operating at high density is attractive for energy-producing future fusion devices. While the density limit in tokamaks is determined largely by the plasma current, this is not true in stellarators, where the magnetic field is provided almost entirely by external coils. The density limit in stellarators is described in first approximation by the empirical Sudo limit [44], $n_{Sudo}[10^{19}\mathrm{m}^{-3}] = 2.5\sqrt{(P_{in}B)/(r^2R)}$, believed to be determined by the balance between the input power and the power radiated by the plasma. Densities above the Sudo density limit are sometimes observed in stellarators, e.g. in LHD [45]. In particular, further studies in LHD and W7-X indicated that the density limit in stellarators might be determined by the power radiated in the edge of the plasma by impurities [45, 46]. On the other hand, recent theory development showed that the density limit in tokamaks might be determined by a transition in edge turbulence [47]. The same mechanism could be at play in stellarators as well.

During boron powder injection experiments, a reduction in intrinsic impurities such as C, O, Fe is generally observed [22], which can result in an overall decrease of the radiated power [32]. Furthermore, during powder injection, a reduction of turbulence and an increase in confinement is sometimes observed [31]. Therefore, B powder injection might result in an increase of the density limit, either in the case it is determined by edge radiation, or edge turbulence, or both. To test this hypothesis, a first set of experiments has been performed in LHD. Here, the density limit is first determined by density ramps. Secondly, the same plasma discharge is repeated, while injecting B powder in the plasma at the same time. Two heating scenarios are considered, a low power one where the plasma is heated by neutral beams $P_{in} = P_{NB} = 3.5$ MW, and a high power one with the addition of electron cyclotron heating $P_{EC} = 1.5$ MW for a total of $P_{in} = P_{NB} + P_{EC} = 5$ MW. In the high power case, for which results are shown in Fig. 12, without B injection a rapid density

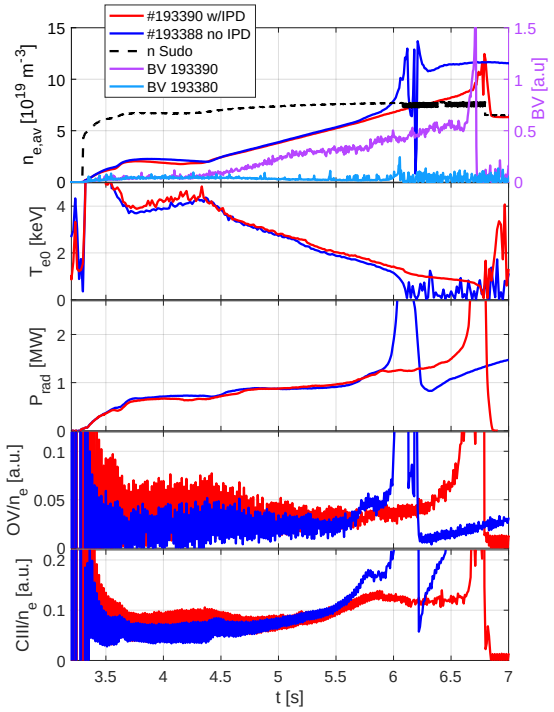

Figure 12: From top to bottom: time traces of electron density and BV spectroscopic measurement, electron temperature, total radiated power, OV and CIII spectroscopic lines normalized to density, for a shot with (red) and without (blue) B powder injection.

increase is observed starting at $n_e \sim 0.85 n_{Sudo}$, quickly leading to a radiative collapse. B powder is injected into the plasma starting at $t = 4.3$ s, in increasing amounts on a shot-to-shot basis. As a result, the maximum attainable density is increased up to $n_e \sim 1.1 n_{Sudo}$. The intrinsic impurity concentration of O and C, measured by the spectroscopic lines OV and CIII respectively, remains below the reference level during B injection. This might be due to a change in neoclassical transport of the impurities. No remarkable change in total radiated power is observed in the phase leading to the collapse of the reference discharge. No substantial change in the density profile is observed as well, while the density fluctuation level measured by phase contrast imaging (PCI) is decreased of 25% in the edge of the plasma $r_{eff}/a_{99} > 0.75$. The turbulence level, for which we consider the line integrated PCI spectrum normalized by the average electron density as a proxy, shows a decrease in the lower frequency part, $F < 30$ kHz, in the phase before the collapse of the reference discharge, $5.5 < t$ [s] < 6, as it is shown in Fig. 13. The turbulence level for higher frequencies, $30 < F[kHz] < 150$, is lower during the first second into powder injection, recovering the reference level in the phase $5.5 < t$ [s] < 6. From here to plasma collapse, the turbulence level in this frequency range is further decreased. The electron temperature is also slightly increased by about 8% as a result of B powder injection, consistently with previous observations of simultaneous turbulence reduction and confinement improvement.
In the lower power case, the reference discharge (without B powder) already reaches a density of $n_e \sim 1.6 n_{Sudo}$. Densities about double the Sudo limit were previously observed in LHD [45]. In this case, the addition of B powder does not result in an increase of the density limit, causing the plasma to collapse slightly earlier instead. The effects of the powder injection observed on the concentration of the intrinsic impurities is mixed, as C concentration is decreased, while O is

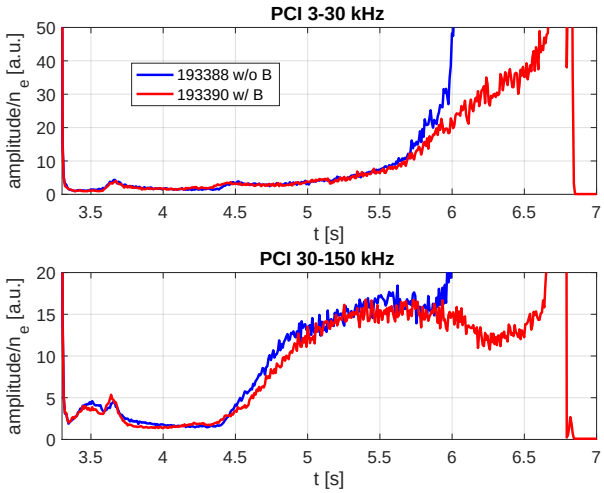

Figure 13: Turbulent density fluctuation amplitude measured by PCI (line integrated) normalized by electron density, for a shot with (red) and without (blue) B powder injection.

increased. The total radiated power is increased by 25%. No substantial change in plasma density and temperature profile is observed during B injection, and the amplitude of the turbulent density fluctuations measured by PCI in the edge of the plasma is increased by $\sim 15\%$ in the phase before the radiative collapse.

This first set of experiments shows encouraging results for improving the density limit via powder injection. Nevertheless, the difference in response between the low and high power scenario needs to be understood. The smaller effect of B powder for the low power scenario might be in part explained with a shallower penetration of the powder and subsequently of the evaporated B ions into the plasma, as the plasma density is higher in this scenario, and the penetration of the powder has been shown to decrease with increased density in LHD due to stronger deflection via ion drag force in the divertor leg, which the powder has to cross to reach the main plasma [15]. The present experiments do not allow us to disentangle the effect of reduced impurity radiation and reduced edge turbulence on the density limit, since both effects occur when B powder injection improves the density limit (high power scenario). Further experiments comparing different powder materials are foreseen for the next LHD campaign to shed light on this matter.

4.2 p-B^{11} fusion

While powder injections experiments have been performed mainly with the goals of improving wall conditions and/or the plasma performances, other applications are possible. As an example, the IPD has the unique capability to provide substantial boron sources to the plasma. The IPD has been instrumental in the realization of a series of experiments aimed at measuring alpha particles born from proton-boron fusion reactions [48]. Here, boron powder is injected with the IPD into plasma heated by 6 MW, 160 kV NBIs. As a preliminary study performed on previous boron powder injection experiments showed, the high energy of the neutral beams results in a substantial number of p-B fusion reactions, enough to be measured at the first wall [49]. A dedicated alpha particle detector was built and dedicated boron powder injection experiments were performed, in which alpha particles born form p-B fusion reactions during powder injection were detected, with good agreement with theoretical models [48].

5 Modeling of powder penetration and boron transport

Numerical simulations have played a fundamental role in the planning and interpretation of impurity powder injection experiments. Simulation with EMC3-EIRENE [50], computing the 3D distribution of plasma quantities in the edge of the plasma, coupled with the DUSTT code [18], computing the trajectory of the powder grains into the plasma, have been used to choose the position to install the IPD on LHD, maximizing the penetration through the ergodic layer among several candidates [14, 15] (Fig. 2). Those simulations also predicted deeper penetration of powder grains into the plasma for lower plasma densities, while at higher plasma densities the plasma flow in the divertor leg is more effective at deflecting their trajectory. Spectroscopic measurements during powder injection experiments later supported this result [19]. Further coupling of EMC3-EIRENE and DUSTT with the ERO2.0 code predicted that the deposition on the wall of B ions resulting from powder injection is more spatially uniform for lower plasma densities, thus making low density plasmas a better candidate for real time wall conditioning applications [21]. EMC3-EIRENE and DUSTT simulations have later been used to interpret the experimental results: by fitting EMC3 simulations to reproduce the experimental profiles, and computing the powder trajectories in such plasmas, it is determined that most of the B powder is evaporated just outside the LCFS [31]. Similar studies have been carried out by coupling EMC3-EIRENE with the DIS code [51] instead, for which composite materials such as BN have been implemented, as well as a statistical treatment of trajectories including a distribution in initial velocities. As a result, most of the BN powder is evaporated in the divertor leg rather than in the main plasma as it is the case for B powder [32]. The EMC3-EIRENE-DUSTT coupling was recently improved by including self consistently the effects of boron ions on the powder trajectories [52], showing how an increase of the amount of injected boron can move the powder ablation point radially inwards due to the cooling of the divertor leg and local reduction of the plasma flow velocity. Finally, the EMC3-EIRENE-DUSTT model was validated against dedicated experiments, reproducing the observed movement of the powder ablation point radially outwards with increasing plasma densities due to the increasing ion drag force in the divertor leg [15]. The EMC3-EIRENE-DUSTT-ERO2.0 model could also qualitatively reproduce the spatial profile of BI and BII line radiation measured from visible spectroscopy, though their variation with plasma density could not be captured by the simulation results so far.

6 Conclusions and outlook

In this article we summarized the powder injection experiments performed in the Large Helical Device in the period 2019-2024 using the Impurity Powder Dropper. The experiments mainly focused on improving the plasma performance, both by improving wall conditions and improving confinement. Injecting boron powder into the LHD plasma has been proven effective in reducing both wall recycling and the influx of intrinsic impurities (C, O, Fe). Wall conditioning effects have been observed both on a shot-to-shot basis due to cumulative B injection, and in real time. Real time wall conditioning by B powder injection has been demonstrated in minutes-long discharges, avoiding an otherwise occurring radiative collapse. These results suggests that real time boronization via powder injection might be an effective way to replenish wall conditions in steady-state operation, but further experiments are needed to demonstrate these capabilities for reactor relevant plasma parameters. Real time wall conditioning has been attempted with different powder materials. Experiments with Si powder did not result in sensible wall conditioning effects, though this could be explained by the fact that this explorative set of experiments were conducted with low power/density plasmas, which were not able to sustain the injection of substantial Si amounts. Li powder wall conditioning experiments have been performed, and the evaluation of the results is still

ongoing and will be the subject of future publications.
Real time wall conditioning via powder injection is an active research topic on both stellarators and tokamaks. Many experiments have been conducted on tokamaks, some examples can be found in references [2, 5, 7, 53, 54, 8, 29]. While a comprehensive review of real time wall conditioning on different devices is outside the scope of this article, similar results have been found across the different machines, with reduction of wall fueling/recycling and concentration of intrinsic impurities during/after low-Z powder injection. The extrapolation of the effectiveness of this technique to future fusion reactors is a topic of growing importance and is currently under investigation. Indeed, fusion reactors are foreseen to operate in steady state for hours at a time, making standard wall conditioning techniques such as glow discharge boronization inconvenient, as they would require to stop plasma operation and turn off the superconducting coils. Furthermore, future fusion reactors are foreseen to operate with high-Z metallic walls, making plasma contamination from intrinsic impurities potentially more deleterious to plasma performance than in current carbon wall machines. The recent decision for ITER to use a full tungsten wall sparked interest in the use of real time wall conditioning for this device as well [11].

The access of a reduced turbulence, improved confinement regime has been observed upon boron powder injection, with increase of the plasma temperature in the order of 25%, but that can be as high as 50% under some conditions. At the same time, the amplitude of the turbulent density fluctuations has been measured by PCI to decrease by up to a factor of 2 in a wide portion of the plasma cross section. The improvement has been observed for both magnetic field directions, different heating schemes, and different main plasma ions (H, D). Series of dedicated experiments have been performed to characterize this improvement, showing how it generally scales positively with the amount of injected B. The relative improvement of the temperature has been found to decrease with both increasing density and input power. The turbulence response though was found to vary in between the different plasma scenarios, possibly depending on the pre-injection turbulence characteristics. Similar effects on confinement and turbulence have been observed with different powder materials such as C, BN and Li. While the reason behind this improvement is not fully understood yet, the most probable explanation is the stabilization of ion scale turbulence, due to the profile and/or Z_{eff} modifications induced by the powder injection. Neoclassical and gyrokinetic simulations partially support this explanation. The improvement of confinement upon powder injection has been leveraged in dedicated experiments to maximize ion temperature in the high T_i scenario, as well as to study impurity transport in turbulence reduced phase.
A similar improvement of confinement upon low-Z powder injection has been observed in W7-X as well [3], where boron carbide B_4C powder was injected horizontally in pulses using the Probe Mounted Powder Injector [9]. Here, a substantial increase of T_i was observed together with a reduction in turbulence. Nevertheless, due to the pulsed nature of the powder injection, the improvement on confinement and T_e, W_p is only transient. More likely the same physical mechanism as the LHD experiments described here are at play in W7-X as well, and a steady state improvement of confinement is expected once the powder is delivered to the plasma as a constant stream. This will be possible with the already planned installation of an IPD on W7-X [10], which is foreseen to be operative in the OP2.4 experimental campaign. Furthermore, a similar increase of confinement upon boron powder injection has been observed for L-mode plasmas in WEST [8, 55], which has been interpreted to be caused by turbulence reduction due to profiles modification [56], similarly to the LHD case. The access to this reduced-turbulence, improved confinement regime appears then to be possible for stellarators and tokamaks alike. While the causes of the observed confinement improvement upon low-Z powder injection are still to be fully understood, and more experiments and modeling work are needed, should this improved confinement regime scale to reactor relevant

scenario, a 25% increase of T_i starting from $T_i = 15$ keV which is the operating point foreseen for future stellarator fusion reactors [57, 58], would increase the D-T reaction rate and energy output by 40%, provided the main ion density can be kept constant.

Boron powder injection was investigated as a possible means of improving the stellarator density limit by reducing radiation from intrinsic impurities and/or edge turbulence, in a first dedicated experiment showing encouraging results. Boron powder has also been injected in LHD plasmas to provide a B source to be used in p-B fusion experiments, successfully measuring for the first time p-B born alpha particles in a magnetic confinement fusion device.
Impurity powder injection experiments are supported by continuous modeling activity of coupled powder dynamics, impurity transport and material migration, helping the interpretation of the experimental results.
Finally, while this article attempted to comprehensively review the impurity powder injection experiments taking place in LHD in the 2019-204 period, several further experiments involving impurity powder injection are planned for the next and last LHD experimental campaign, taking place at the end of 2025. These new experiments will help further improving the understanding of the topics exposed in this article, such as real time wall conditioning with different powder materials and its application to steady-state discharges, the access to a reduced turbulence improved confinement regime via low-Z powder injection, the effect of low-Z powders on the density limit, and more generally impurity transport in a stellarator plasma.

Acknowledgments

The authors wish to thank the LHD experiment group for the excellent support of this work, and Drs. R. Seki and M. Yokoyama (NIFS) for executing TASK3D-a suite, allowing to conduct transport analyses. The authors thank Dr. Y. Feng from Max-Planck Institute for Plasma Physics, Dr. D. Reiter from Heinrich-Heine University Düsseldorfand, and Dr. R. Smirnov from UCSD Plasma Theory Group for granting the permission to use the EMC3, EIRENE and DUSTT codes, respectively. This work was conducted within the framework of the NIFS/PPPL International Collaboration, and it is supported by the U.S. DOE under Contract No. DE-AC02-09CH11466 with Princeton University.

Data availability

The datasets of the Large Helical Device (LHD) described in these proceedings are available in the LHD data repository server of the National Institute for Fusion Science (NIFS) at
`https://doi.org/10.57451/lhd.analyzed-data`

References

[1] J. Winter. **Wall conditioning in fusion devices and its influence on plasma performance**. *Plasma Physics and Controlled Fusion*, **38**:1503, 1996.

[2] A. Bortolon et al. **Observations of wall conditioning by means of boron powder injection in DIII D H-mode plasmas**. *Nuclear Fusion*, **60**:126010 1–13, 2020.

[3] R. Lunsford, C. Killer, A. Nagy, D. Gates, T. Klinger, A. Dinklage, S. Lazerson, F. Nespoli, N. A. Pablant, G. Satheeswaran, et al. . **Characterization of injection and confinement**

improvement through impurity induced profile modifications on the Wendelstein 7-X stellarator. *Physics of Plasmas*, **28**:082506, 2021.

[4] A. Nagy et al. **A multi-species powder dropper for magnetic fusion applications**. *Review of Scientific Instruments*, **89**:10K121, 2018.

[5] R. Lunsford , V. Rohde, A. Bortolon , R. Dux, A. Herrmann, A. Kallenbach , R.M. McDermott , P. David, A. Drenik, F. Laggner, R. Maingi, D. K. Mansfield, A. Nagy, R. Neu, E. Wolfrum and the ASDEX Upgrade team. **Active conditioning of ASDEX Upgrade tungsten plasma-facing components and discharge enhancement through boron and boron nitride particulate injection**. *Nuclear Fusion*, **59**:126034, 2019.

[6] Z. Sun et al. **Suppression of edge localized modes with real-time boron injection using the tungsten divertor in EAST**. *Nuclear Fusion*, **61**:014002 1–8, 2021.

[7] E.P. Gilson al. . **Wall Conditioning and ELM Mitigation with Boron Nitride Powder Injection in KSTAR**. *Nuclear Materials and Energy*, **28**:101043, 2021.

[8] G. Bodner et al. **Initial results from boron powder injection experiments in WEST lower single null L-mode plasmas**. *Nuclear Fusion*, **62**:086020, 2022.

[9] A. Nagy et al. **A horizontal powder injector for W7-X**. *Fusion Engineering and Desing*, **146**:1403–1407, 2019.

[10] F. Nespoli et al. **Numerical modeling of impurity powder injection in W7-X**. *Nuclear Materials and Energy*, **42**:101837, 2025.

[11] J.A. Snipes et al. **Initial design concepts for solid boron injection in ITER**. *Nuclear Materials and Energy*, **41**:101809, 2024.

[12] Y. Yoshimura et al. **Achievement of One Hour Discharge with ECH on LHD**. *Journal of Physics: Conference Series*, **25**:189, 2005.

[13] Y. Yoshimura et al. **Progress of long pulse discharges by ECH in LHD**. *Nuclear Fusion*, **56**:046005, 2016.

[14] M. Shoji, G. Kawamura, R. Smirnov, Y. Tanaka, S. Masuzaki, Y. Uesugi, N. Ashikawa, E. Gilson, R. Lunsford. **Full-torus impurity transport simulation for optimizing plasma discharge operation using a multi-species impurity powder dropper in the large helical device**. *Contributions to Plasma Physics*, :e201900101, 2019.

[15] M. Shoji et al. **Full-torus impurity transport simulation in boron powder injection experiments in the Large Helical Device**. *Nuclear Materials and Energy*, **41**:10180, 2024.

[16] Y. Feng et al. **3D Edge Modeling and Island Divertor Physics**. *Contributions to Plasma Physics*, **44**:57 – 69, 2004.

[17] G. Kawamura et al. **First EMC3-EIRENE Simulations with Divertor Legs of LHD in Realistic Device Geometry**. *Contributions to Plasma Physics*, **54**:437 – 441, 2014.

[18] R.D. Smirnov, A Yu Pigarov, M Rosenberg, S I Krasheninnikov and D A Mendis. **Modelling of dynamics and transport of carbon dust particles in tokamaks**. *Plasma Physics and Controlled Fusion*, **49**:347–371, 2007.

[19] F. Nespoli, N. Ashikawa, E.P. Gilson, R. Lunsford, S. Masuzaki, M. Shoji, T. Oishi, C. Suzuki, A. Nagy, A. Mollen, N.A. Pablant, K. Ida, M. Yoshinuma, N. Tamura, D.A. Gates, T. Morisaki, the LHD experiment group . **First impurity powder injection experiments in LHD**. *Nuclear Materials and Energy*, **25**:100842, 2020.

[20] T. Oishi et al. **Line identification of boron and nitrogen emissions in extreme- and vacuum-ultraviolet wavelength ranges in the impurity powder dropping experiments of the Large Helical Device and its application to spectroscopic diagnostics**. *Plasma Science and Technology*, **23**:084002 1–12, 2021.

[21] M. Shoji et al. **Boron transport simulation using the ERO2.0 code for real-time wall conditioning in the large helical device**. *Nuclear Materials and Energy*, **25**:100853, 2020.

[22] R. Lunsford et al. **Real-time wall conditioning and recycling modification utilizing boron and boron nitride powder injections into the Large Helical Device**. *Nuclear Fusion*, **62**:086021, 2022.

[23] N. Ashikawa et al. **Coated boron layers by boronization and a real-time boron coating using an impurity powder dropper in the LHD**. *Plasma Science and Technology*, **26**:085103, 2024.

[24] T. Kawate et al. **Experimental study on boron distribution and transport at plasma-facing components during impurity powder dropping in the Large Helical Device**. *Nuclear Fusion*, **62**:126052 (9pp), 2022.

[25] S. Masuzaki et al. **Impact of boron powder dropping on helium plasma in LHD**. *25TH PSI Conference, South Korea*, page P163(C), 2022.

[26] S. Masuzaki et al. **Glow Discharge Boronization and Real-Time Boronization Using an Impurity Powder Dropper in LHD**. *Nuclear Materials and Energy*, **42**:101843, 2025.

[27] V. Rohde et al. **Comparison of Boronization and Siliconization in ASDEX Upgrade**. *26th EPS Conf. on Contr. Fusion and Plasma Physics, Maastricht, 14 - 18 June 1999*, 1999.

[28] G.Z. Zuo et al. **Comparison of various wall conditionings on the reduction of H content and particle recycling in EAST**. *Plasam Physics and Controlled Fusion*, **54**:015014, 2012.

[29] F. Effenberg et al. **In-situ coating of silicon-rich films on tokamak plasma-facing components with real-time Si material injection**. *Nuclear Fusion*, **63**:106004, 2023.

[30] S. Zamperini et al. **SiC as a core-edge integrated wall solution in DIII-D**. *Nuclear Materials and Energy*, **37**:101535, 2023.

[31] F. Nespoli et al. **Observation of a reduced-turbulence regime with boron powder injection in a stellarator**. *Nature Physics*, **18**:350–356, 2022.

[32] F. Nespoli et al. **A reduced-turbulence regime in the Large Helical Device upon injection of low-Z materials powders**. *Nuclear Fusion*, **63**:076001, 2023.

[33] M. Yokoyama et al. **Extended capability of the integrated transport analysis suite, TASK3D-a, for LHD experiment**. *Nuclear Fusion*, **57**:126016 1–7, 2017.

[34] G. Motojima et al. **Particle control in long-pulse discharge using divertor pumping in LHD**. *Physica Scripta*, **97**:035601, 2022.

[35] M. Landreman al. **Comparison of particle trajectories and collision operators for collisional transport in nonaxisymmetric plasmas**. *Physics of Plasmas*, **21**:042503, 2014.

[36] T. Singh et al. **Global gyrokinetic simulations of electrostatic microturbulent transport in LHD stellarator with boron impurity**. *Nuclear Fusion*, **64**:016007, 2024.

[37] M. Nunami et al. **Linear Gyrokinetic Analyses of ITG Modes and Zonal Flows in LHD with High Ion Temperature**. *Plasma and Fusion Research*, **6**:1403001, 2011.

[38] T. Kinoshita et al. **Turbulence Transition in Magnetically Confined Hydrogen and Deuterium Plasmas**. *Physical Review Letters*, **132**:235101, 2024.

[39] K. Ida et al. **Overview of Large Helical Device experiments of basic plasma physics for solving crucial issues in reaching burning plasma conditions**. *Nuclear Fusion*, **64**:112009, 2024.

[40] J.M. Garcia-Regana et al. **Reduction or Enhancement of Stellarator Turbulence by Impurities**. *Physicsl review Letters*, **133**:105101, 2024.

[41] D. Medina-Roque et al. **Impact of Li-powder injection on the improvement of bulk energy and particle transport and expulsion of mid/high-Z impurities in high-density plasmas in LHD**. *Physical Review Letters*, :submitted, 2025.

[42] S. Buller et al. **The importance of the classical channel in the impurity transport of optimized stellarators**. *Journal of Plasma Physics*, **85**:175850401, 2019.

[43] H. Takahashi et al. **Progress in extending the high-temperature pl 1 asma regime in the LHD**. *Journal of Fusion Energy*, :submitted, 2025.

[44] S. Sudo et al. **Scalings of energy confinement and density limit in stellarator/heliotron devices**. *Nuclear Fusion*, **30**:11, 1990.

[45] J. Miyazawa et al. **Density limit study focusing on the edge plasma parameters in LHD**. *Nuclear Fusion*, **48**:015003, 2008.

[46] G. Fuchert et al. **Increasing the density in Wendelstein 7-X: benefits and limitations**. *Nuclear Fusion*, **60**:036020, 2020.

[47] M. Giacomin et al. **First-Principles Density Limit Scaling in Tokamaks Based on Edge Turbulent Transport and Implications for ITER**. *Physicsl review Letters*, **128**:185003, 2022.

[48] R. Magee et al. **First measurements of p^{11}B fusion in a magnetically confined plasma**. *Nature Communications*, **14**:955, 2023.

[49] K. Ogawa et al. **Evaluation of Alpha Particle Emission Rate Due to the p-^{11}B Fusion Reaction in the Large Helical Device**. *Fusion Science and Technology*, **78**:175–185, 2022.

[50] Y. Feng et al. **Recent Improvements in the EMC3-Eirene Code**. *Contributions to Plasma Physics*, **54**:426 – 431, 2014.

[51] F. Nespoli et al. **Impurity seeding for suppression of the near scrape-off layer heat flux feature in tokamak limited plasmas**. *Physics of Plasmas*, 25:052501, 2018.

[52] M. Shoji et al. **Self-consistent transport simulation of boron dust particle injection in the peripheral plasma in Large Helical Device**. *Contributions to Plasma Physics*, :e202300105, 2024.

[53] Z. Sun et al. . **Real time wall conditioning with lithium powder injection in long pulse Hmode plasmas in EAST with tungsten divertor**. *Nuclear Materials and Energy*, **19**:124–130, 2019.

[54] A. Schamis et al. **Wall conditioning effects of boron powder injection in KSTAR with a tungsten divertor**. *Nuclear Fusion*, **65**:086037, 2025.

[55] R. Lunsford et al. **Plasma modification through boron particulate injection in the full tungsten environment of WEST**. *Nuclear Fusion*, **65**:106009, 2025.

[56] G. Bodner et al. **Stability analysis of WEST L-mode discharges with improved confinement from boron powder injection**. *Plasma Physics and Controlled Fusion*, **66**:045022, 2024.

[57] J. Lion et al. **Stellaris: A high-field quasi-isodynamic stellarator for a prototypical fusion power plant**. *Fusion Engineering and Design*, **214**:114868, 2025.

[58] C. Hegna et al. **The Infinity Two Fusion Pilot Plant baseline plasma physics design**. *Journal of Plasma Physics*, :doi:10.1017/S0022377825000364, 2025.